Summing coincidence in rare event γ-ray measurements under an ultra-low background environment

L.-C. He[a], L.-J. Diao[b], B.-H. Sun[a,*], L.-H. Zhu[a,*], J.-W. Zhao[a], M. Wang[a], K. Wang[a]

[a] *School of Physics and Nuclear Energy Engineering, Beihang University, Beijing 100191, People's Republic of China*

[b] *China Institute of Atomic Energy, Beijing 102413, People's Republic of China*

Abstract

Full-energy peak (FEP) efficiencies of a HPGe detector equipped with an ultra-low background shield system are calibrated with the Monte Carlo method and further examined using summing peaks in a numerical way. Radionuclides ^{241}Am, ^{137}Cs, ^{60}Co, ^{133}Ba and ^{152}Eu are used to construct the simulation model with the toolkit GEANT4. True summing coincidence factors (TSCFs) of ^{60}Co, ^{133}Ba and ^{152}Eu are calculated and result in an improvement up to about 20% in the FEP efficiency curve. Counts of summing coincidence γ peaks in the spectra of ^{60}Co and ^{152}Eu can be well reproduced using the corrected efficiency curve within an accuracy of 3%.

Keywords: HPGe detector, ultra-low background shield system, summing coincidence, GEANT4

1. Introduction

γ-ray spectroscopies using high-purity germanium (HPGe) detectors are widely applied in radiation measurements due to the excellent energy resolution. Moreover, low-background detection shields are developed to suppress the interference from environmental radiations during accurate measurements for extreme low-activity samples [1]. A precision calibration of the detection efficiency are crucial for a reliable measurement of low-activity samples. Usually standard sources such as ^{133}Ba and ^{152}Eu are used for the calibration purpose [2]. However, one difficulty here is that cascade gamma-rays in these sources would result in true summing coincidences during measurements due to the short distance between the source and the detector and the narrow space inside the shielding system [3].

When two or more γ rays emitted from the radionuclide are detected within the time resolution of a detector, the true summing coincidence takes place, i.e., these two or more γ rays would be summed and mistaken as one. In recent years, Monte Carlo simulations have been used to correct the summing coincidences [4, 5, 6]. High accurate simulation models of detectors had to be built with a number of monoenergetic

*Corresponding author

Email addresses: bhsun@buaa.edu.cn (B.-H. Sun), zhulh@buaa.edu.cn (L.-H. Zhu)

sources, basically more than 5, to calculate true summing coincidence factors (TSCFs) and full-energy peak (FEP) efficiencies in the study energy range. Alternatively, calculations based on numerical expressions can also provide TSCFs for radionuclides [7]. Even spectra of complex decay scheme such as ^{152}Eu can be predicted in this way [8]. Both methods have their certain restrictions: the first method has to rely on the model optimization with data of monoenergetic sources, while the numerical approach is hard to extend to cases with complex geometries such as volumetric sources and materials besides the detector.

In the present work, we attempt to reduce the dependence of the simulation on monoenergetic sources and meanwhile maintain the accuracy of the model. Two monoenergetic point sources ^{241}Am and ^{137}Cs, and standard point sources ^{60}Co, ^{133}Ba and ^{152}Eu are used to construct a Monte Carlo simulation model of the HPGe detector with the shield system. The toolkit GEANT4 [9, 10, 11] is adapted to reproduce the effect of shield materials around the detector, from which the scattered or induced photons can take part in summing coincidences. Moreover, to inspect the FEP efficiency we have developed a numerical approach to calculate the counts of the summing peaks of cascade γ rays.

This paper is organized as follows. In Section 2, we introduce our experimental set up. In Section 3, the construction of the simulation model and the calculation of TSCFs are illustrated, the result of the FEP efficiency calibration is presented as well. Section 4 contains the discussion of our calculation and our numerical examination method with summing peaks. Finally, the conclusion is summarized in Section 5.

2. Experiments

Measurements were taken using a HPGe detector equipped with an ultra-low background shield system. The detector is an ORTEC GEM series p-type coaxial HPGe detector with a 0.9 mm thick carbon-fiber window [12]. The relative efficiency is 105% at 1.33 MeV (active volume around 400 cm^3) and the energy resolution is 1.84 keV at 1.332 MeV. The ultra-low background shield system consists of an outer support chamber made of lead and steel, plastic scintillator detectors, a cadmium absorber, an inner lead ring and an oxygen-free copper liner. A schematic view of the whole detector is shown in Fig. 1. Lead shields are designed to eliminate most of the low energy background and the plastic scintillator detectors to veto cosmic rays. The copper liner surrounding the detector can absorb γ-induced X-rays from lead. Inside shields is filled with nitrogen to remove radioactivity from the radon in air. The main parameters of the HPGe detector and the shield system are summarised in Table 1.

The anti-coincidence circuit for signals from cosmic rays is set up using the SCA function of a time-to-amplitude converter (TAC) model. It can generate anti-coincidence signals according to time correlations of start signals from the HPGe detector and stop signals from the plastic scintillators. The logic schematic is shown in Fig. 2. If the time difference of two signals is between the preset upper and lower thresholds, the SCA output will generate a anti-coincidence signal to veto the HPGe signal from the cosmic ray. The TAC model provides an easy adjustment of the anti-coincidence circuit.

The whole detector system provides an overall background of 0.1 counts per second.

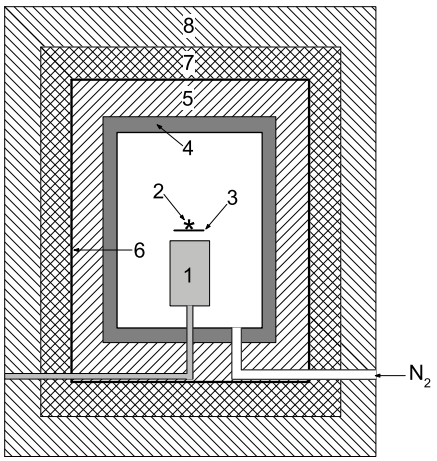

Figure 1: Schematic of the ultra-low background measurement system containing a HPGe detector with 105% relative efficiency. 1 is the HPGe detector, 2 the source, 3 the ABS plastic holder, 4 the copper liner, 5 the inner lead ring, 6 the cadmium absorber, 7 the plastic scintillator, and 8 the outer chamber.

A multi-channel analyzer of 16384 channels with ORTEC software MAESTRO version 7 [13] was used to record data. A mixed standard point source composed of ^{60}Co, ^{137}Cs and ^{241}Am and two point sources ^{133}Ba and ^{152}Eu were used in measurements. Table 2 lists the activities of different sources and live measurement times respectively. All these standard sources are placed on an ABS plastic holder with thickness of 2.5 mm and 22.1 mm away from the surface of the detector. The measured γ-ray spectra are shown in Fig. 3 with black lines, from which the counts of FEPs have been deduced with a γ-ray spectroscopy analysis software Radware [14].

3. FEP efficiency and correction of TSCF

3.1. FEP efficiency

The FEP efficiency of the HPGe detector, ε, can be calculated by the following equation:

$$\varepsilon = \frac{N}{tAB_{\gamma}}F_{tsc}, \qquad (1)$$

where N is the net counts of FEPs, t the live time of measurements, A the source activity, B_{γ} the branching ratio of specific gamma ray and F_{tsc} the true summing coincidence factor.

Generally, if the distance between the source and the detector surface is long enough with respect to the size of the detector surface and there is no other objects surrounding the detector which would lead to γ scattering or γ induced photons, the parameter F_{tsc} can be ignored and treated as 1 in Eq. (1). Consequently, the FEP efficiencies without correction are extracted from the measurement spectra and shown in Fig. 4 (a).

A Polynomial function in the log-log scale is usually used to describe the relationship between the FEP efficiency and the γ energy. However, in order to show the influence of absorber before the detector, we use the EFFIT program in Radware package, a standard approach, to describe the efficiency curve [14]. The FEP efficiency curve is presented in Fig. 4 (a) with the dash line

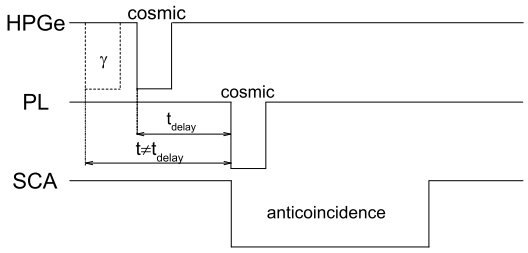

Figure 2: Logic schematic of anti-coincidence circuit. HPGe, PL and SCA are the time signals from the HPGe detector, plastic scintillator and the SCA output of the time-to-amplitude converter (TAC) model respectively. For details, refer to the text.

Table 1: Dimensions of HPGe detector and ultra-low background shield system

	Component	Dimension (mm)
HPGe	Crystal diameter	85
	Crystal length	79.8
	Lithium diffused depth	∼0.7
	Hole diameter	9
	Hole depth	66.2
	Carbon fiber window thickness	0.9
	Detector surface to crystal surface	7
Shields	Outer chamber thickness	115
	Plastic scintillator thickness	100
	Cadmium absorber thickness	1
	Inner lead ring thickness	75
	Copper liner thickness	25
	Copper liner diameter	180
	Copper liner length	500

Table 2: Characteristics of standard sources used in measurements

No.	Nuclide	activity (kBq)	Live time(s)
1	^{241}Am	5.96 (10)	1000
	^{137}Cs	1.07 (2)	
	^{60}Co	1.45 (2)	
2	^{133}Ba	29.4 (6)	300
3	^{152}Eu	19.0 (4)	600

and the fitting function used is:

$$\begin{aligned}\varepsilon_\gamma =& exp\{[(a+bx+cx^2)^{-g} \\ &+(d+ey+fy^2)^{-g}]^{-1/g}\},\end{aligned} \quad (2)$$

in which $x = log(E_\gamma/E_1)$ and $y = log(E_\gamma/E_2)$, E_1=100 keV, E_2=1000 keV and E_γ is in keV. Seven parameters of function from a to g are fitted from the data.

An obvious fluctuation of data points around the curve can be seen in Fig. 4 (a). This is due to the distance of the source to the detector is only 22.1 mm in our measurements and the shield materials are too close to the detector, resulting in an enhanced true summing coincidences. Therefore, the correction of the true summing coincidence factor is necessary for the FEP efficiency calibration in our case.

3.2. Correction of TSCF

TSCF is defined as [6] the ratio of the real FEP efficiency to the uncorrected efficiency calibrated using radionuclides as mentioned in Section 3.1. Ideally the real FEP efficiency can be obtained with monoenergetic sources experimentally. However, it is practically impossible to find enough monoenergetic sources covering the whole energy region of interest. On the other hand, both FEP efficiencies with and without the true summing coincidence correction can be ob-

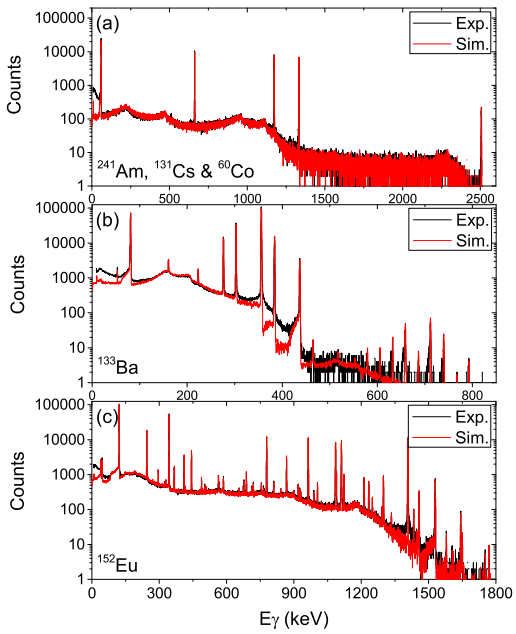

Figure 3: Comparison of experimental (black) and simulated (red) spectra for (a) a mixed source of ^{60}Co, ^{137}Cs and ^{241}Am, (b) ^{133}Ba and (c) ^{152}Eu. Statistics of simulation are set to be the same as the relevant measurements.

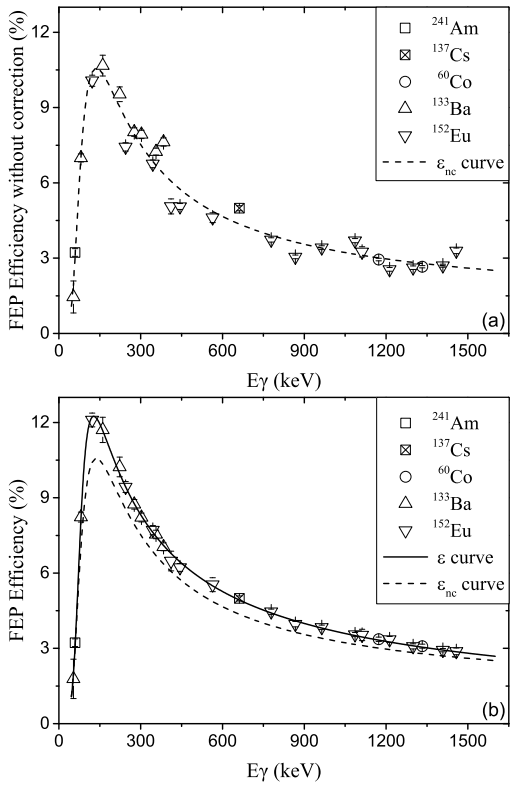

Figure 4: FEP efficiency curve fitted using experimental data without (a) and with (b) the true summing coincidence correction. Data of monoenergetic radionuclides ^{241}Am and ^{137}Cs are presented with squares, and nuclides contain true summing coincidence, ^{60}Co, ^{133}Ba and ^{152}Eu are shown with dots and triangles. The dash curve in (b) is the same as the curve in (a).

tained using a well constructed Monte Carlo simulation model. In this way, the true summing coincidence factor (F_{tsc}) can be calculated by the equation:

$$F_{tsc} = \frac{\varepsilon_{sim}^{mono}}{\varepsilon_{sim}^{nc}}, \qquad (3)$$

where ε_{sim}^{mono} is the simulated real FEP efficiency obtained with the isotropic monoenergetic γ rays, and ε_{sim}^{nc} is the simulated FEP efficiency without correction using various radionuclides. This is the basic idea of the correction in our work.

3.2.1. Simulation data basis and physics processes

Simulations in the present work are performed using the GEANT4 program version 10.2. Data libraries applied to the simulations are listed as follow:

1) G4EMLOW version 6.41 [11], which describes low energy electromagnetic (EM) processes for photon, electron or positron, muon, hadron or ion, X-ray and polarized electron and gamma beams.

2) G4RadioactiveDecay version 4.3.2 [11], which includes radioactive decay hadronic processes based on ENSDF data [15] and nuclear wallet cards [16].

The physics constructor class of G4EmStandardPhysics_option4 [11] is used in simulations [17]. Physical process of Rayleigh scattering, fluorescence, Auger electron, nuclear stopping, accurate

angular generator for ionisation models and bremsstrahlung for secondary particles are included. To enable the simulation of low energy physical processes especially for the γ induced photon emission from materials, the model construction has done the invocation of threshold energies for each material and for each particle type (i.e. electron and gamma).

In addition, to reproduce the energy response of the detector, a random Gaussian fluctuation is added to each energy deposition generated by GEANT4. For a HPGe detector, its energy resolution can be described as:

$$R_{FWHM} = p_1\sqrt{E_\gamma} + p_2. \qquad (4)$$

With R_{FWHM} and E_γ extracted from the experimental spectra, p_1 and p_2 can be obtained and further used for the Gaussian fluctuation of the energy deposition. The toolkit ROOT [18] is used to sort the data into spectra event by event.

3.2.2. Model construction

Simulation model of GEANT4 is established based on geometries. Since there is no external background, only the inner copper liner of the shield system is reserved in the construction, other components are neglected to improve the computation speed. The germanium crystal and the hole inside are constructed as cylinders and shields as tubs. However, the thickness of the dead layer in HPGe crystal and the active volume in HPGe crystal can not be determined directly due to the aging of the detector and the condition of the power supply. Instead, these two unknown parameters, which have great influence to the FEP efficiency, can be effectively adjusted according to experimental spectra.

The model was constructed by the following three steps:

1) The thickness of the dead layer and the diameter of the active volume are tentatively assigned first to the approximate values, using which the simulation can reproduce fairly the experimental FEP efficiencies at 59.5 keV and 661.7 keV from the monoenergetic sources ^{241}Am and ^{137}Cs. This is due to the diameter of the active volume affects FEP efficiencies at all the energy region, while the thickness of the dead layer mainly impacts the FEP efficiency at the low energy ($<$ 200 keV). In this step, the thickness of the dead layer was refined at 1.3 ± 1 mm and the diameter of the active volume 80 ± 3 mm.

2) For further adjustments, the experimental spectra of ^{60}Co and ^{133}Ba have to be used. ^{60}Co provides the efficiency information at energies more than 1 MeV, and ^{133}Ba at energies from 53.2 to 383.8 keV. ^{133}Ba is important to constrain the most dramatic changing region of the HPGe FEP efficiency curve. To get the value of the dimensions as accurate as possible, the parameters of the dead layer and the active crystal diameter are varied at a step of 0.01 mm and 0.1 mm respectively. The optimized values of 1.27 mm and 80.8 mm are eventually obtained.

3) Spectrum of ^{152}Eu, with a wider energy spectrum from 121.8 keV to 1408.0 keV, is further used as a cross check of the parameters determined in the previous two steps. In case needed, further adjustments are possible by repeating the steps above.

Using the well adjusted model, 27 main simulated FEP efficiencies without correction, ε^{nc}_{sim}, are obtained and shown with experimental data, ε^{nc}_{exp}, in Table 3. Only statistic errors are considered here. Note the 81.00-keV γ ray of ^{133}Ba in the table actually corresponds to the unresolved 79.61-

and 81.00-keV γ rays and the 443.96-keV γ ray of ^{152}Eu the unresolved 443.96- and 444.0-keV γ rays.

As seen in Table 3, all the uncorrected efficiencies determined from the experimental data and simulations are fully consistent within standard deviations. The largest relative deviation of efficiency is 3.18% and the mean value of relative deviations is 1.40%.

The simulated spectra for different radionuclides are shown in Fig. 3 compared with the experimental spectra. The statistics of simulations are set to be the same as measurements according to the activities and live measurement times in Table 2. The spectrum of the mixed source of ^{60}Co, ^{137}Cs and ^{241}Am is simply the sum of spectrum of each nuclide. All the peaks on experimental spectra even with very weak intensities can be well reproduced, except the low-energy region of less than 100 keV and around 400 keV in Fig. 3 (b) and 1400 keV in (c). We will address these discrepancies later in Section 4.

3.2.3. Efficiency with TSCF correction

Using the model constructed above the FEP efficiencies with and without the correction are obtained, and F_{tsc} for ^{60}Co, ^{133}Ba and ^{152}Eu are calculated with Eq. (3). The FEP efficiencies with correction and F_{tsc} are presented in Table 3.

The FEP efficiency curve fitted with the experimental data after the correction is presented in Fig. 4(b). Different from the one without the correction, all the data points are much more consistent with the curve. The true summing coincidence clearly leads to an underestimation of most FEPs' intensities from ^{60}Co, ^{133}Ba and ^{152}Eu, with a maximum relative deviation up to around 20%. This shows the necessity to have a precise and reliable evaluation of the summing coincidence in the process of efficiency calibration.

4. Discussion

4.1. Accidental coincidence

Beside the true summing coincidences, accidental coincidences can be seen in our measurements due to high activities of radioactive sources. The evidence is the low statistic peaks at energy more than 500 keV in Fig. 3 (b), which is higher than the highest level (437.0 keV) in the decay scheme of ^{133}Ba and come from the summation of γ rays emitted by two ^{133}Ba nuclei in accidental coincidences. To reproduce these peaks, simulations are performed using the set of two radionuclides decaying simultaneously in one event. Comparing the counts of pure accidental coincidence peaks in simulations to the experimental ones, the double accidental coincidence rate of ^{133}Ba are determined to be 3.5% and ^{152}Eu to be 2.7%. Triple or higher accidental coincidences can be safely ignored in agreement with experimental measurements. Note that the accidental coincidences are already considered in the correction of TSCF.

4.2. Failure of anti-coincidence circuit

Fig. 5 shows the zoomed spectrum of ^{152}Eu. Discrepancies can be found at the platform of energy region of less than 100 keV and around the peak of 1408.0 keV. Similar situations can also be seen in other spectra, especially the one of ^{133}Ba in Fig. 3 (b).

One of the possible reasons of these discrepancies is the failure of the anti-coincidence circuit which may lead to mistake signals from cosmic rays. As mentioned in Section 2, the SCA function of a time-to-amplitude converter (TAC) model

Table 3: Measured (ε^{nc}_{exp}) and simulated (ε^{nc}_{sim}) uncorrected FEP efficiencies, the true summing coincidence factors (F_{tsc}), and FEP efficiencies after TSCF corrections (ε).

Nuclei	E_γ (keV)	ε^{nc}_{exp} (%)	ε^{nc}_{sim} (%)	F_{tsc}	ε (%)
^{241}Am	59.5409	3.23 (15)	3.26 (15)	1	3.23 (15)
^{137}Cs	661.657	4.99 (10)	4.89 (10)	1	4.99 (10)
^{60}Co	1173.228	2.95 (5)	2.98 (5)	1.14 (2)	3.37 (9)
	1332.492	2.66 (5)	2.69 (5)	1.16 (2)	3.09 (8)
^{133}Ba	53.1622	1.5 (6)	1.47 (5)	1.23 (3)	1.8 (8)
	80.9979	6.99 (16)	6.95 (15)	1.177 (10)	8.2 (2)
	160.612	10.7 (4)	10.6 (3)	1.10 (2)	11.7 (5)
	223.2368	9.5 (3)	9.4 (3)	1.07 (2)	10.2 (4)
	276.3989	8.03 (17)	8.07 (17)	1.089 (7)	8.74 (19)
	302.8508	7.93 (16)	8.00 (16)	1.036 (6)	8.22 (17)
	356.0129	7.24 (14)	7.13 (14)	1.041 (12)	7.54 (17)
	383.8485	7.63 (16)	7.62 (16)	0.924 (6)	7.05 (16)
^{152}Eu	121.7817	10.1 (2)	9.8 (2)	1.202 (8)	12.1 (3)
	244.6974	7.44 (17)	7.49 (17)	1.268 (7)	9.4 (2)
	344.2785	6.76 (15)	6.66 (15)	1.141 (8)	7.71 (18)
	411.1165	5.1 (3)	5.2 (3)	1.281 (15)	6.5 (4)
	443.9606	5.06 (12)	5.15 (12)	1.231 (12)	6.22 (16)
	563.986	4.6 (2)	4.56 (14)	1.20 (3)	5.5 (3)
	778.9045	3.73 (8)	3.69 (8)	1.197 (8)	4.46 (10)
	867.38	3.05 (7)	3.15 (8)	1.300 (14)	3.97 (11)
	964.057	3.42 (8)	3.44 (8)	1.123 (7)	3.84 (9)
	1085.837	3.70 (8)	3.72 (8)	0.960 (7)	3.55 (8)
	1112.076	3.3 (2)	3.2 (2)	1.087 (11)	3.5 (2)
	1212.948	2.55 (7)	2.50 (7)	1.31 (3)	3.36 (12)
	1299.142	2.62 (7)	2.67 (7)	1.17 (2)	3.08 (10)
	1408.013	2.70 (6)	2.77 (6)	1.086 (8)	2.93 (7)
	1457.643	3.29 (11)	3.36 (11)	0.88 (3)	2.88 (14)

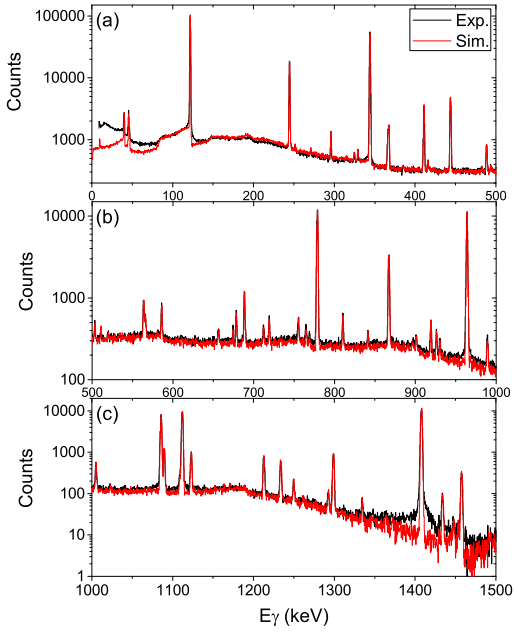

Figure 5: Comparison of experimental (black) and simulated (red) spectrum of source ^{152}Eu at three different energy region.

is used for the anti-coincidence circuit. However, the time correlation of signals in the TAC may be disrupted, which then fail to give the anti-coincidence signals while the counting rate of the HPGe detector is too high. As seen in Fig. 2 with dash lines, if the start sinal of the TAC is firstly triggered by the γ signal from the source, the time difference of two signals may be out of the preset upper and lower thresholds. Consequently, no anti-coincidence signal is generated and the signal in the HPGe detector from the cosmic ray will be recorded. Such effect is apparently shown in the low energy region. Furthermore, if these signals from cosmic rays have coincidences with full absorbed γ rays, the shape of the γ peaks would be effected as seen in Fig. 5 (c) at the energy of 1408 keV.

The effect induced by cosmic rays could affect, in general, the low energy region but barely for the counts of FEPs at energies of interest and also the calculation of TSCFs. Therefore, such effect was not considered in the simulation model.

4.3. TSCF evaluation with summing peaks

True summing coincidences of full absorbed cascade γ rays can result in new summing peaks in spectra, which do not correspond to any γ rays in decay schemes. However, counts of these peaks can be predicted precisely based on the known decay schemes, FEP efficiencies and angular correlations between cascade γ rays with a numerical way. By comparing with real experimental counts, it is possible to examine FEP efficiencies determined.

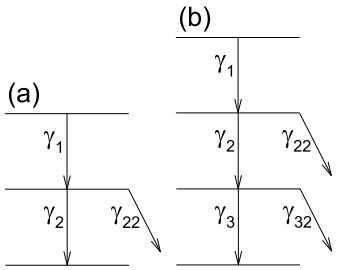

Figure 6: Schematic of (a) the two-sequential cascade γ-ray transition and (b) the three-sequential cascade γ-ray transition

For a two-sequential cascade transition, γ_1 and γ_2, where γ_1 is followed by γ_2 as seen in Fig. 6 (a), the counts of the summing peak of γ_1 and γ_2, N_{cal}, is:

$$N_{cal} = tAB_{\gamma_1}P_{\gamma_2}\int_0^{\Omega_{det}}\int_0^{\Omega_{det}}\frac{\eta_{\gamma_1}}{4\pi}\frac{\eta_{\gamma_2}}{4\pi}W(\theta)d\Omega_1 d\Omega_2, \quad (5)$$

where t is the live time of the measurement, A the activity of the source, B_{γ_1} the branching ratio of γ_1. P_{γ_2} is the emission probability of γ_2 from its initial level which equal to the branching ratio of γ_2 divided by the sum of branching ratios of γ_2 and

γ_{22} $(B_{\gamma_2}/(B_{\gamma_2}+B_{\gamma_{22}}))$, Ω_{det} the solid angle of the detector, η_{γ_1} and η_{γ_2} the intrinsic efficiencies of the detector, $W(\theta)$ the directional correlation, θ the angle between γ_1 and γ_2, and $d\Omega_1 d\Omega_2$ integration elements of solid angles corresponding to different emission directions of γ_1 and γ_2.

In Eq. (5), the FEP efficiency for each γ ray is described with the solid angle of the detector and the intrinsic efficiency of each γ ray:

$$\varepsilon_\gamma = \int_0^{\Omega_{det}} \eta_\gamma \frac{1}{4\pi} d\Omega = \frac{\Omega_\gamma}{4\pi}. \qquad (6)$$

The intrinsic efficiency, η_γ, depends on the energies, emission directions and thicknesses of the HPGe crystal on the directions, and is difficult to calculate. In first order, here we use a nominal conical solid angle, Ω_γ, to represent the combination of Ω_{det} and η_γ ($\Omega_\gamma = \int_0^{\Omega_{det}} \eta_\gamma d\Omega$). Then the size of the nominal detection solid angle of each γ ray can be deduced by FEP efficiencies.

Consequently, the Eq. (5) can be wrote as:

$$\begin{aligned} & N_{cal} \\ =& tAB_{\gamma_1}P_{\gamma_2}\int_0^{\Omega_{\gamma_1}}\int_0^{\Omega_{\gamma_2}} \frac{1}{4\pi}\frac{1}{4\pi} W(\theta) d\Omega_1 d\Omega_2 \\ =& tAB_{\gamma_1}P_{\gamma_2}\varepsilon_{\gamma_1}\varepsilon_{\gamma_2}\frac{\int_0^{\Omega_{\gamma_1}}\int_0^{\Omega_{\gamma_2}} W(\theta) d\Omega_1 d\Omega_2}{4\pi\varepsilon_{\gamma_1} 4\pi\varepsilon_{\gamma_2}} \\ =& tAB_{\gamma_1}P_{\gamma_2}\varepsilon_{\gamma_1}\varepsilon_{\gamma_2}C_{ac}, \end{aligned} \qquad (7)$$

where ε_{γ_1} and ε_{γ_2} are the corrected FEP efficiencies of γ_1 and γ_2, and they can be obtained from the corrected efficiency curve. C_{ac} corresponds to the correction factor of the angular correlation.

The directional correlation, $W(\theta)$, is computed as:

$$W(\theta) = \sum_\nu A_\nu^{(1)} A_\nu^{(2)} P_\nu(cos\theta), \qquad (8)$$

where P_ν are the even Legendre polynomials, i.e., the summation is over the even integers including zero. The $A_\nu^{(1)}$ and $A_\nu^{(2)}$ depend only on the spins and multipolarities of the first and second transitions of the cascade, respectively, and are already tabulated in, e.g., Ref., textbook [19].

Moreover, we can extend the equation to three-sequential cascade γ-ray transitions $(\gamma_1 - \gamma_2 - \gamma_3)$ as Fig. 6 (b):

$$N_{cal} = tAB_{\gamma_1}P_{\gamma_2}P_{\gamma_3}\varepsilon_{\gamma_1}\varepsilon_{\gamma_2}\varepsilon_{\gamma_3}C_{ac_{12}}C_{ac_{23}}, \qquad (9)$$

where P_{γ_3} is the emission probability for the third γ ray, $C_{ac_{12}}$ and $C_{ac_{23}}$ represent the correction factor of the angular correlation between adjacent cascade γ rays, $\gamma_1 - \gamma_2$ and $\gamma_2 - \gamma_3$, respectively.

Numerical calculations were applied to simple $\gamma-\gamma$ cascade of ^{60}Co and some summing peaks at energies of levels which do not have direct transitions to the ground state on the spectrum of ^{152}Eu [20]. Summarized in Table 4 are the results of the calculations and experimental counts of summing peaks. As seen in the table, the 1643.4-keV and 1123.2-keV summing peaks mainly come from respective two-sequential cascade of γ-ray transitions, the 1649.8-keV summing peak mainly from three two-sequential cascades, and the 1579.5-keV summing peak mainly from one two-sequential cascade and one three-sequential cascade. Other cascades not mentioned in the table are negligible in the calculations due to their relatively very weak branching ratios or emission probabilities.

N_{cal} and N_{exp} in Table 4 are well consistent within statistical errors. Counts of summing peaks are well reproduced and the γ rays involved in calculations cover most of the energy regions of the FEP efficiency curve. This verifies the correction of our ef-

Table 4: Comparison of numerical calculations and experimental measurements for counts of summing coincidence γ peaks in spectra of ^{60}Co and ^{152}Eu.

Decay	E_{sum} (keV)[a]	E_γ (keV)[b]	E_i (keV)[c]	E_f (keV)[d]	C^e_{ac}	N^f_{cal}	N^g_{exp}
^{60}Co→60Ni	2505.7	1173.2	2505.7	1332.5	1.09	1595	1622 (43)
		1332.5	1332.5	0			
^{152}Eu→^{152}Gd	1643.4	1299.1	1643.4	344.3	1.20	508	509 (27)
		344.3	344.3	0			
^{152}Eu→^{152}Gd	1123.2	778.9	1123.2	344.3	0.95	4532	4611 (80)
		344.3	344.3	0			
^{152}Eu→^{152}Sm	1649.8	1528.1	1649.8	121.8	1.15	112	115 (12)
		121.8	121.8	0			
		686.6	1649.8	963.4	1.04		
		963.4	963.4	0			
		564.0	1649.8	1085.8	1.19		
		1085.8	1085.8	0			
^{152}Eu→^{152}Sm	1579.5	1457.6	1579.5	121.8	1.19	114	112 (12)
		121.8	121.8	0			
		1213.0	1579.5	366.5	1.05		
		244.7	366.5	121.8	&		
		121.8	121.8	0	0.91		

[a]Energies of summing peaks.
[b]Energies of γ rays involved.
[c]Excitation energies of initial levels.
[d]Excitation energies of final levels.
[e]Correction factors for angular correlations.
[f]Counts of summing peaks from calculations.
[g]Counts of summing peaks extracted from experimental spectra.

ficiency calibration for the detector system.

5. Conclusion

The FEP efficiency calibration of a HPGe detector equipped with an ultra-low background shield system has been performed using standard point sources and a Monte Carlo simulation. The simulation model is established with spectra of radionuclides ^{241}Am, ^{137}Cs, ^{60}Co, ^{133}Ba and ^{152}Eu using the toolkit GEANT4. It was found that introducing the TSCF correction resulted in a up to about 20% improvement to the FEP efficiency curve. Furthermore, with this improved efficiency curve the summing peaks in the spectra of ^{60}Co and ^{152}Eu, which were not used in the model construction, can be nicely reproduced in a numerical way. This demonstrates the robust of the present simulation.

Acknowledgment: This work is partially supported by the National Natural Science Foundation of China (Grants No. 11375023, No. 11575018, No. 11475014) and National Key Research and Development Program (Grant No. 2016YFA0400500).

References

[1] L. Trnková, P. Rulík, Low background shielding of HPGe detector, Appl. Radiat. Isot., 67 (2009) 723-725.

[2] R. G. Helmer, Efficiency calibration of a Ge detector for 30-2800 keV γ rays, Nucl. Instrum. Methods Phys. Res. A, 193 (1982) 87-90.

[3] Klaus Debertin, Ulrich Sch¨tzig, Coincidence summing corrections in Ge(Li)-spectrometry at low source-to-detector distances, Nucl. Instrum. Methods, 158 (1979) 471-477.

[4] M. Décombaz, J.-J. Gostely, J.-P. Laedermann, Coincidence summing corrections for extended sources in gamma-ray spectrometry using Monte Carlo simulation, Nucl. Instrum. Methods Phys. Res. A, 312 (1992) 152-159.

[5] S. Dziri, A. Nourreddine, A. Sellam, A. Pape, E. Baussan, Simulation approach to coincidence summing in γ-ray spectrometry, Appl. Radiat. Isot., 70 (2012) 1141-1144.

[6] G. Giubrone, J. Ortiz, S. Gallardo, et al., Calculation of Coincidence Summing Correction Factors for an HPGe detector using GEANT4, J. Environ. Radioact., 158-159 (2016) 114-118.

[7] S. Rizzo, E. Tormachio, Numerical expressions for the computation of coincidence-summing correction factors in gamma-spectrometry with HPGe detectors, Appl. Radiat. Isot., 85 (2010) 555-560.

[8] Dragana Jordanov, et al., The application of the new matrix method for calculating coincidence summing effects in the case of radionuclide with the more complex decay scheme - ^{152}Eu, Nucl. Instrum. Methods Phys. Res. A, 836 (2016) 22-29.

[9] S. Agostinelli, J. Allison, K. Amako, et al., GEANT4-a simulation toolkit, Nucl. Instrum. Methods Phys. Res. A, 506 (2003) 250-303.

[10] J. Allison, K. Amako, J. Apostolakis, et al., Geant4 developments and applications, Nuclear Science IEEE, 53 (2006).

[11] J. Allison, K. Amako, J. Apostolakis, et al., Recent developments in GEANT4, Nucl. Instrum. Methods Phys. Res. A, 835 (2016) 186-303.

[12] ORTEC INDUSTIES, High Purityu Germanium (HPGe) Radiation Detectors, available at http://www.ortec-online.com/products/radiation-detectors/germanium-hpge-radiation-detectors

[13] ORTEC INDUSTIES, MAESTRO Multichannel Analyzer Emulation, available at http://www.ortec-online.com/products/application-software/GammaVision.pdf.

[14] RadWare, available at http://radware.phy.ornl.gov/

[15] Evaluated Nuclear Structure Data File (ENSDF), available at http://www.nndc.bnl.gov/ensdf

[16] Nuclear Wallet Cards, available at http://www.nndc.bnl.gov/wallet

[17] D. Cullen, J.H. Hubbell, L. Kissel, The Evaluated Photon Data Library, Report UCRL-50400, vol. 6 (1997).

[18] R. Brun, F. Rademakers, Root - an object oriented data analysis framework, Nucl. Instrum. Methods Phys. Res. A, 389 (1997) 81-86.

[19] Kai Siegbahn, α-, β- and γ-ray spectroscopy, 1965.

[20] Richard B. Firestone, Table of Isotopes. Version 1.0. 1996.